VOLUME 111, NUMBER 4
FEBRUARY 15, 1989

JOURNAL
OF THE
AMERICAN
CHEMICAL
SOCIETY

Laser Ion Beam Photodissociation Studies of Model Amino Acids and Peptides

R. E. Tecklenburg, Jr., M. N. Miller, and D. H. Russell*

Contribution from the Department of Chemistry, Texas A&M University, College Station, Texas 77840. *Received June 9, 1988*

Abstract: Visible (458–514.5 nm) and UV (333–385 nm) photodissociation of the $[M + H]^+$ ions of dinitrophenyl (DNP) derivatized amino acids and peptides is reported. Photoexcitation of the DNP peptides by a visible photon results in fragmentation of the peptide chain with little fragmentation within the chromophore. Conversely, UV photoexcitation of the DNP peptides results in fragmentation of the chromophore as well as the peptide chain, but loss of NO or NO_2 (within the chromophore) often dominates the photofragment ion spectrum. These results are rationalized with particular emphasis on "energy-selective" dissociation channels of large ionic systems. DNP-leucine and DNP-isoleucine $[M + H]^+$ can be differentiated on the basis of photodissociation reactions which yield distonic radical cations. The rate of dissociation of photoexcited ions of DNP peptides is shown to decrease with increasing molecular weight (degrees of freedom). Lastly, comparisons between photodissociation and collision-induced dissociation as a structural probe are presented.

Tandem mass spectrometry has become an important analytical tool for identification and structural characterization of complex molecules. The use of tandem mass spectrometry in conjunction with fast atom bombardment (FAB) ionization[1] has many advantages for structural characterization of large bimolecules (m/z = 1000–2000 amu), especially problems related to sensitivity and sample purification.[2,3] The intrinsic advantages for the combined use of FAB and tandem mass spectrometry is that the molecular ion, e.g., $[M + H]^+$, $[M - H]^-$, etc., of a thermally labile, polar molecule can be formed, and the mass-selected $[M + H]^+$ or $[M - H]^-$ ion can be subjected to collision-induced dissociation (CID). Structural information for the $[M + H]^+$ or $[M - H]^-$ ion can then be inferred from the collision-induced dissociation spectrum. Extension of the FAB tandem mass spectrometry technique to the analysis of bimolecules >2000 amu is currently limited by poor sensitivities. Limitations in the MS-MS experiment can be attributed to at least three factors: (i) FAB ionization yields for $[M + H]^+$ and $[M - H]^-$ ions decrease as a function of the molecular weight of the sample, (ii) the CID of large bimolecules often lack structurally significant fragment ions (i.e., small stable neutral losses dominate the daughter ion spectra), and (iii) the efficiency for production of CID fragment ions is reduced for high mass ions. The limited efficiency for production of CID product ions has been attributed to the collisional activation process[4] as well as the dissociation dynamics of large molecules.[5]

The ion internal energy distributions and energy transfer accompanying CID of high molecular weight species is not well understood. Few studies exist on the factors influencing CID efficiencies of large polyatomic ions, as well as the fundamental aspects of the collisional activation and subsequent dissociation processes. Derrick et al. studied the CID product ion yields as a function of molecular weight for a series of peptides (m/z 400–1600) and proposed that the increased energy uptake accompanying collisional activation and the reduced CID efficiencies at high mass result from limitations in the dissociation dynamics. That is, the average energy deposited per vibrational mode by collisional activation is too small to induce fragmentation for large ions which have high numbers of degrees of freedom. Although the degrees-of-freedom effect on CID efficiencies is no doubt

(1) Barber, M.; Bordoli, R. S.; Elliott, G. J.; Sedgwick, R. D.; Tyler, A. N. *Anal. Chem.* **1982**, *54*, 645A.
(2) Blemann, K.; Martin, S. A. *Mass Spectrom. Rev.* **1987**, *6*, 1.
(3) Jensen, N. J.; Gross, M. L. *Mass Spectrom. Rev.* **1987**, *7*, 1.
(4) Bricker, D. L.; Russell, D. H. *J. Am. Chem. Soc.* **1986**, *108*, 6174.
(5) Neumann, G. M.; Shell, M. M.; Derrick, P. J. *Z. Naturforsch* **1984**, *39a*, 584.

0002-7863/89/1511-1161$01.50/0

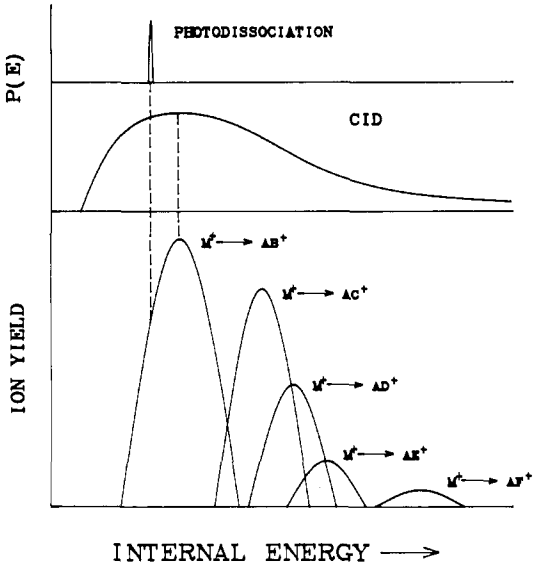

Figure 1. A hypothetical breakdown graph for the M^+ ion as a function of internal energy.

important, other processes competitive with collisional activation must be considered.[4,6] For example, recent studies on the 8-keV CID of chlorophyll *a* ions on various monatomic target gases were interpreted as evidence that endothermic charge-transfer reactions have large cross sections.[4] These studies point out an intrinsic limitation of the collisional activation process; specifically, a significant fraction of the total energy loss accompanying collisional activation is due to energy transfer to the target gas as opposed to internal energy deposition into the incident ion.

Photodissociation offers an alternative to CID for the study of ion activation/dissociation and the structural characterization of complex molecules.[6,7] Because photodissociation involves interaction of an ion with a photon (as opposed to a particle in CID), translational energy loss that accompanies collisional activation is not observed, thereby eliminating ambiguity in the amount of internal energy deposited into the incident ions as well as the mass assignments of product ions.[4,5] Although photodissociation has been extensively used to study the dissociation dynamics and fundamental properties of small gas-phase ions,[8-10] few reports exist on the utility of the method for identification and characterization of large polyatomic ions.[11,12] Unlike CID, photoexcitation yields an ion population with a narrow range of internal energies. Typical energy deposition functions, $P(E)$, for collisional activation and photodissociation and a hypothetical energy breakdown graph for a complex polyatomic ion are depicted in Figure 1. The broad distribution of internal energies resulting from collisional activation,[13] generally results in an ion population which yields large numbers of fragment ions. On the other hand, the narrow distribution of internal energies deposited by photoexcitation is expected to result in a limited number of observed photodissociation reaction channels (e.g., only the AB^+ fragment ion will be observed by photodissociation at the low photon energies depicted in Figure 1). A larger variety of photofragment ions will be observed in cases where substantial overlap between reaction channels exist, e.g., the energy range where $M^+ \rightarrow AC^+$ and $M^+ \rightarrow AD^+$ overlap.

In this paper, we present the results of performing photodissociation for a series of derivatized amino acids and di- and tripeptides. Derivatized peptides were used for these studies because: (i) laser-ion beam photodissociation is limited by the requirement for a laser system with high average power, specifically a high-power CW laser (e.g., Ar ion laser with emission lines in the low-energy UV (333–365 nm) and visible blue-green (454–514.5 nm) region;[7] (ii) peptides do not absorb in the wavelength range of the laser system; thus photoexcitation is accomplished by attaching a UV-visible chromophore to the peptide. An important side issue of this study is the role of charge-site versus remote-charge-site directed dissociation.[14] For example, in each model system photoexcitation occurs at the dinitrophenyl chromophore, but the charge-carrying portion of the ion is the peptide.[15,16] Thus, photoexcitation, and possibly dissociation, occurs remote from the charge site. Whether separation of the initial site of excitation and charge will alter the dissociation reactions of the ion will depend upon the dissociation dynamics. For instance, if the chromophore has a low-energy photochemical reaction channel (either dissociation or rearrangement), then this reaction could be the dominant decay channel. The dinitrophenyl group has two relatively low-energy dissociation channels, loss of NO and NO_2 (electron impact appearance energies of ca. 3 and 2.0–2.5 eV, respectively, above the ionization threshold).[17] Thus, photoexcitation by 454–514.5-nm photons (2.73–2.41 eV) yields ions with sufficient internal energy for loss of NO_2. Because the photoexcited ion (2.73–2.41-eV internal energy) lies near the threshold for NO_2 loss, the ion may be relatively long-lived and dissociation reactions with similar energy requirements should be competitive. However, the competition between reaction channels with similar energy requirements will be determined by the frequency factors for the two reaction channels, i.e., kinetic effects. Conversely, photoexcitation by low-energy UV (ca. 3.5 eV) could produce a photoexcited ion sufficiently short-lived that NO_2 (or even NO) loss is the dominant decay channel. The strong dependence of ion yields on internal energy and the narrow internal energy distributions of the photoexcited ions could lead to dramatic differences (both in terms of the product ions formed and relative abundance) between the CID and photodissociation spectra.

Although photodissociation may develop as an important method for structural characterization of complex molecules,[18] our studies are designed to understand the underlying factors that influence dissociation. The systems selected for these studies contain a dinitrophenyl group (DNP) and the DNP group is attached to the N-terminus of the amino acids and peptides.

Experimental Section

A schematic diagram of the experimental apparatus used for the present studies is shown in Figure 2. The Kratos MS-50 TA laser-ion beam photodissociation apparatus has been described in detail in an earlier paper.[19] Briefly, the first electrostatic analyzer and magnetic analyzer comprise a high-resolution MS-I (R = 150000)[20] for mass selection of a particular ion, and ion activation (via photons or collisions with a neutral target) is performed in the third field-free region of the mass spectrometer. The second electrostatic analyzer (MS-II) is then used for kinetic energy analysis of the fragment ions. The kinetic energy of the fragment ions can be related to the mass-to-charge ratio by the relationship; $m_2^+ = m_1^+(E_2/E_1)$, where m_2^+ is the m/z value of the

(6) Fukuda, E. K.; Campana, J. E. *Anal. Chem.* **1985**, *57*, 949.
(7) Beynon, J. H.; Brenton, A. G.; Harris, F. M. *Int. J. Mass Spectrom. Ion Phys.* **1982**, *45*, 5.
(8) Dunbar, R. C. *Gas Phase Ion Chemistry*; Bowers M. T., Ed.; Academic Press: New York, 1979; Vol. 2, p 181.
(9) Harris, F. M.; Beynon, J. H. *Gas Phase Ion Chemistry, Ions and Light*; Bowers, M. T., Ed.; Academic Press: Orlando, FL, 1984; Vol. 3, Chapter 19, p 99.
(10) Krailler, R. E.; Russell, D. H.; Jarrold, M. F.; Bowers, M. T. *J. Am. Chem. Soc.* **1985**, *107*, 2346.
(11) Hunt, D. F.; Shabanowitz, J.; Yates, J. R., III *J. Chem. Soc., Chem. Commun.* **1987**, 548.
(12) Watson, C. H.; Baykut, G.; Eyler, J. R. *Anal. Chem.* **1987**, *59*, 1133.
(13) Cooks, R. G. In *Collison Spectroscopy*, Cooks, R. G., Ed.; Plenum Press: New York, 1978; pp 363–377.
(14) Tomer, K. B.; Crow, F. W.; Gross, M. L. *J. Am. Chem. Soc.* **1983**, *105*, 5487.
(15) Biemann, K.; Martin, S. A. *Mass Spectrom. Rev.* **1987**, *6*, 1.
(16) Russell, D. H.; McGlohon, E. S.; Mallis, L. M. *Anal. Chem.* **1988**, in press.
(17) Morgan, R. P.; Beynon, J. H.; Bateman, R. H.; Green, B. N. *Int. J. Mass Spectrom. Ion Phys.* **1978**, *28*, 171.
(18) Hunt, D. F.; Shabanowitz, J.; Yates, J. R., III *J. Chem. Soc., Chem. Commun.* **1987**, 548.
(19) Tecklenburg, R. E., Jr.; Russell, D. H. *J. Am. Chem. Soc.* **1987**, *109*, 7654.
(20) Gross, M. L.; Chess, E. K.; Lyon, P. A.; Crow, F. W.; Evans, S.; Tudge, H. *Int. J. Mass Spectrom. Ion Phys.* **1982**, *42*, 243.

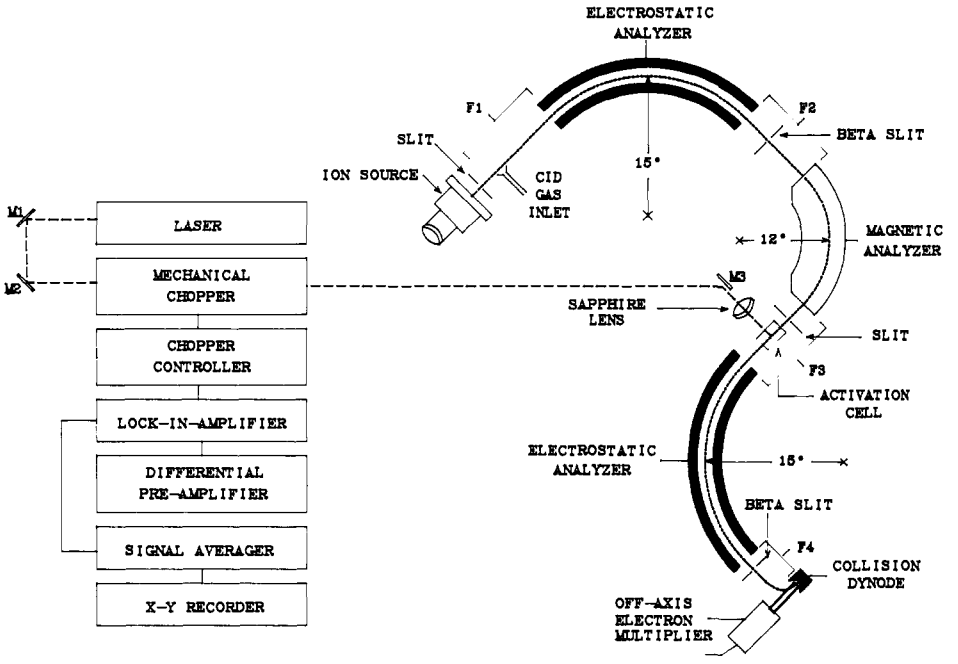

Figure 2. Schematic diagram of the laser-ion beam photodissociation apparatus. The laser beam (dashed line) is perpendicularly overlapped with the ion beam in the third field-free region of the mass spectrometer.

fragment ion, m_1^+ is the m/z value for the incident ion, E_2 is the electrostatic analyzer voltage necessary to pass m_2^+, and E_1 is the electrostatic analyzer voltage necessary to pass m_1^+. Ion detection is performed by using an off-axis post acceleration detector.

Ions are produced in an fast-atom bombardment (FAB) source using an Ion Tech 11-NF fast-atom saddle field gun; 10 μA of Xe neutral beam current (as indicated by the Ion Tech FAB gun cathode current) was maintained at the high-voltage cathode (6–7 kV) of the FAB gun. The photodissociation studies were performed by using the blue-green (458–514.5 nm; 2.4–2.7 eV) and UV (333–385 nm; 3.2–3.7 eV) lines of a CW argon ion laser (Coherent Model CR-18). Mirrors M1, M2, and M3 (see Figure 2) are used to direct the laser beam through a sapphire window in the center of the third field-free region where the laser beam and ion beam are crossed in an orthogonal fashion. A 300-mm focal length sapphire lens is used to focus the laser beam to a small point (0.1–0.3 mm in diameter) just at the laser-ion beam intersection in the center of the activation cell. Photodissociation is performed within 1 cm of the image focal point of MS-I, where the dimensions of the ion beam are small (<0.25 mm). Photofragment ions formed between the magnetic analyzer and second electrostatic analyzer are energy analyzed using standard mass-analyzed kinetic energy (MIKE) scans.[21-23] The laser beam is mechanically chopped at a frequency of 400 Hz, and the photofragment ion signal is separated from the metastable and the collision-induced product ions by using a lock-in amplifier (Princeton Applied Research Model 124A) which measures laser "on"/laser "off" difference signal. The difference signal is then accumulated and signal-averaged. The stored averaged spectra are plotted using a Houston Instrument Series 2000 X-Y recorder.

The times required for ions to undergo photodissociation are measured in the present study using a biased activation cell.[24] The activation cell has been modified for the purpose of performing photodissociation experiments by addition of two 0.8-mm holes at the center of the cell. These holes serve as entrance and exit ports for the laser beam. In addition, the output of the tunable high-voltage power supply (±0–8 kV) has been connected to the electrically isolated activation cell. This allows the cell to be biased with respect to the adjacent lenses. Figure 3 is an expanded view of the third field-free region of the mass spectrometer which contains the activation cell. When the activation cell is biased by a voltage V', the cell acts as a symmetric Einsel lens, decelerating and accelerating the ions as they enter and exit the cell, respectively. Thus,

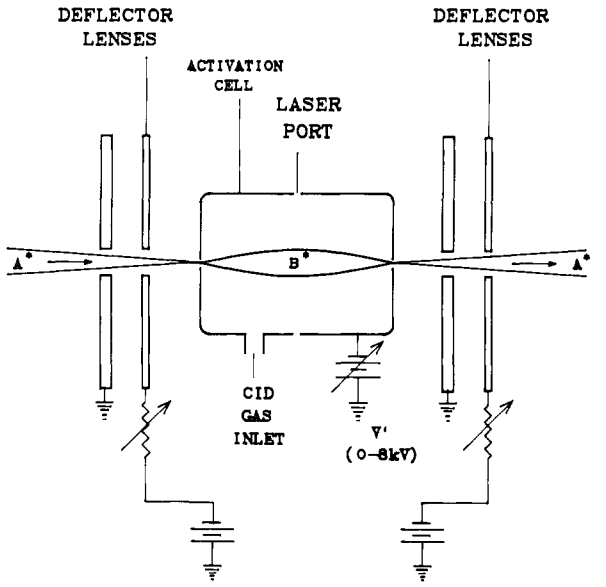

Figure 3. Expanded view of the third field-free region of the mass spectrometer which contains the biased activation cell.

ions which undergo photodissociation within the biased activation cell are shifted in kinetic energy with respect to metastable ions dissociating outside the cell. Positive ions dissociating within the biased activation cell (B*) have a kinetic energy defined by $[(m_2/m_1)V + (1 - (m_2/m_1)V']$,[25] while ions dissociating outside the cell (A*) have a kinetic energy defined by $[(m_2/m_1)V]$, where V is the main beam accelerating voltage and V', the biased cell voltage. The advantages of the biased activation cell for photodissociation studies are that (i) significant fractions (>90%) of metastable noise can be separated from the photodissociation signal, thus increasing signal-to-noise ratios, and (ii) measurements of the proportion of ions that photodissociate within the cell (prompt dissociation) to outside the cell (slow dissociation) can be made. This latter advantage allows the rates of photofragmenting ions to be estimated from a knowledge of the lengths of the activation cell (1.9 cm) and field-free region (40.6 cm) and the velocities of the ions within these regions. For example, photodissociation rates of $>5.6 \times 10^6$ s^{-1} and $5.6–0.286 \times 10^6$ can be specified for a 500-amu ion ($V = 8$ kV, $V' = 1$ kV) photodissociating within and outside the activation cell, respectively. In addition,

(21) Cooks, R. G.; Beynon, J. H.; Caprioli, R. M.; Lester, G. R. *Metastable Ions*; Elsevier: Amsterdam–London–New York, 1973.
(22) Gross, M. L.; Russell, D. H. *Tandem Mass Spectrometry*; McLafferty, F. W., Ed.; Wiley: New York, 1983; p 255.
(23) Russell, D. H.; Smith, D. H.; Warmack, R. J.; Bertram, L. K. *Intg. J. Mass Spectrom. Ion Phys.* **1980**, *35*, 381.
(24) Tecklenburg, R. E., Jr.; Sellers Hann, M. L.; Russell, D. H., submitted to *Int. J. Mass Spectrom. Ion Proc.*
(25) Morgan, R. P.; Beynon, J. H.; Bateman, R. H.; Green, B. N. *Int. J. Mass Spectrom. Ion Phys.* **1978**, *28*, 171.

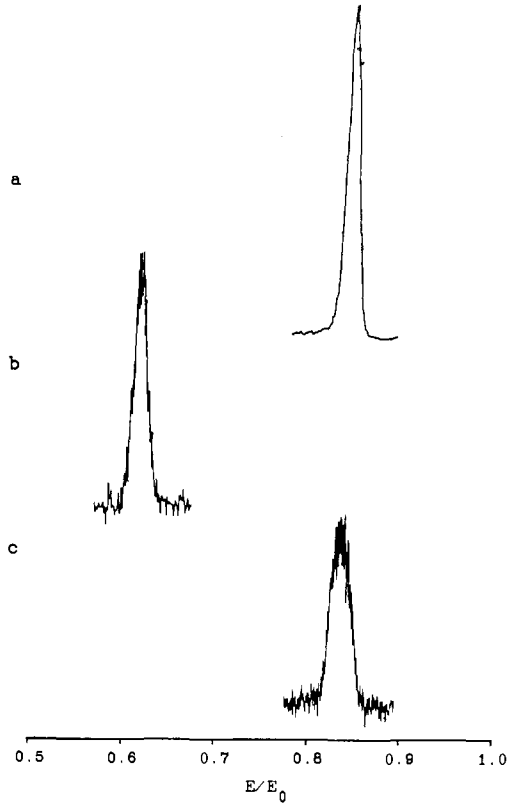

Figure 4. Photofragment ion signals for a selected DNP amino acid, DNP dipeptide, and DNP tripeptide. The ratio E/E_0 corresponds to the m/z ratio for the photofragment and precursor ions: (a) signal for loss of COOH• (m/z 298 → 252) from DNP-leucine $[M + H]^+$; (b) signal for the A_1 cleavage (m/z 313 → 197)of the DNP-glyala $[M + H]^+$; (c) signal for the B_2 cleavage (m/z 454 → 379) of the DNP-Pro-Leu-Gly $[M + H]^+$. All data collected by using the "all-lines" visible wavelengths (ca. 22 W) with 32 signal-averaged scans.

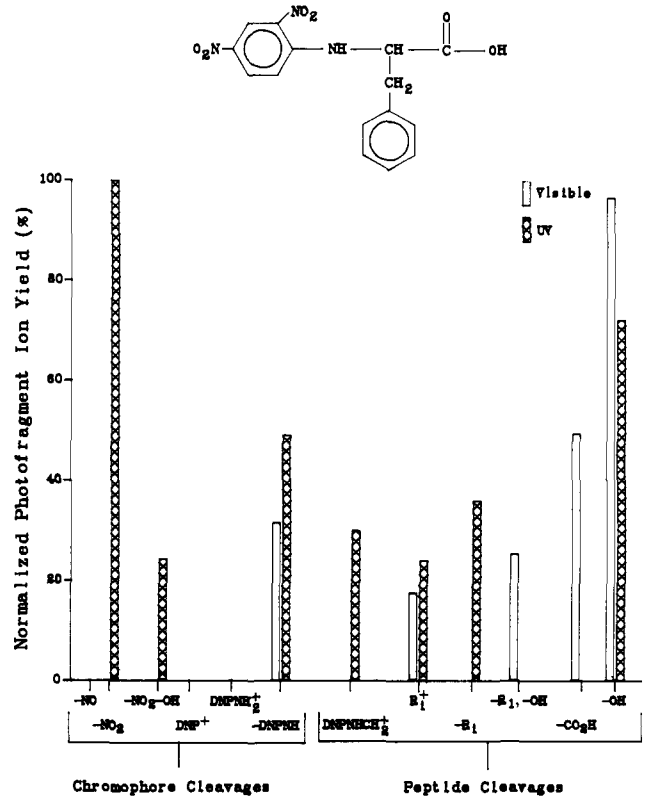

Figure 5. Photofragment ion histogram of DNP-phenylalanine. Photodissociation at visible and UV wavelengths are represented by open and cross-hatched bars, respectively.

ions dissociating entirely within the activation cell will be kinetic energy shifted with respect to ions that dissociate outside the activation cell.

Dinitrophenyl derivatized peptides were purchased from Chemical Dynamics Corp., (South Plainfield, NJ 07080); nitrobenzyl alcohol, glycerol, and methanol were purchased from Aldrich Chemical Co. (Milwaukee, WI 53201). Solutions of each peptide were prepared by dissolving 1 mg of each peptide into 10 mL of HPLC grade methanol. These solutions were then diluted 1:100 on a stainless steel FAB probe tip with nitrobenzyl alcohol or glycerol. Because no measurable impurities were observed in the mass spectra of these compounds, the samples were used without purification.

Results

This work investigates the visible and low-energy UV single-photon photodissociation of dinitrophenyl derivatized amino acids and peptides. The dinitrophenyl (DNP) group or Sanger's reagent attached to the N-terminus of the peptide serves as a visible and low-energy UV chromophore. From previous work in this laboratory we know that the DNP group has a large absorption cross section at 365 nm and in the blue-green region between 458 and 514.5 nm (weaker absorption than 365 nm by ca. five times; consistent with solution UV–vis absorption spectral data for model peptides).[26] The results of these solution-phase studies also find the absorption spectra of DNP peptides to be independent of the composition of the peptide. In addition, the absorption transitions at >300 nm are due exclusively to the DNP group and, to a first approximation, are independent of pH.

Tables I–III summarize the photofragment ion yields for the 14 DNP amino acids and peptides examined in this paper. Photofragment ion signals for selected reactions are contained in Figure 4. The reported photofragment ion yields (I) are normalized to the transition having the largest photodissociation cross section. The tables also contain the percentage of the total ion current each photodissociation reaction channel represents ($(I/\Sigma I) \times 100$). For the sake of comparison, collision-induced dissociation and metastable ion data are also reported in Tables I–III. Although complete CID and metastable ion spectra are not reported, the relative intensities (I) and percent total ion current ($I/\Sigma I$) for CID and metastable reaction channels common to photodissociation are reported. Thus, comparisons can be made as to the relative importance of the various reaction channels by the different activation methods.

Selected photofragment ion histograms are reported for dinitrophenyl derivatized amino acids and peptides in Figures 5–8. Note that these figures contain relative abundance data for visible (open bars) and UV photodissociation (cross-hatched bars), The cleavage reactions are grouped into two categories; (i) chromophore cleavages which consist of structurally nonsignificant fragment ions within or adjacent to the DNP chromophore, e.g., loss of NO, NO_2, and formation of DNP^+ or $DNPNH_2^+$; and (ii) peptide cleavages which consists of structurally significant fragment ions (A_i, B_i, ...) and cleavage reactions which involve the side chain and the C-terminus, e.g., loss of R, CO_2H, or OH, etc. Peptide sequence ions observed in the photofragment ion spectra of peptides are reported using the nomenclature proposed by Roepstorff[27] (see structure I).

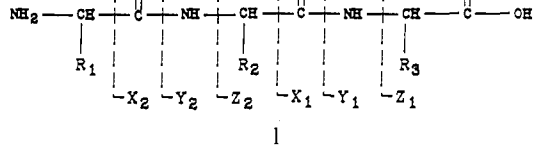

I

Tables I–III also contain kinetic data for the photodissociation reactions, specifically the percentage prompt dissociation for each

(26) Miller, M. N. M.S. Thesis, Texas A&M University, College Station, TX 77843, 1987.

(27) Roepstorff, P. *Biomed. Mass Spectrom.* **1984**, *11*, 601.

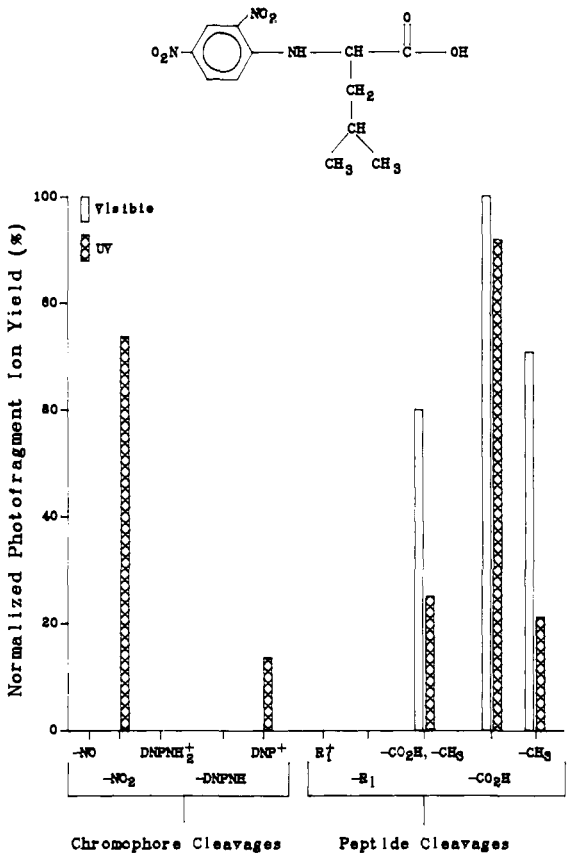

Figure 6. Photofragment ion histogram of DNP-leucine. Photodissociation at visible and UV wavelengths are represented by open and cross-hatched bars, respectively.

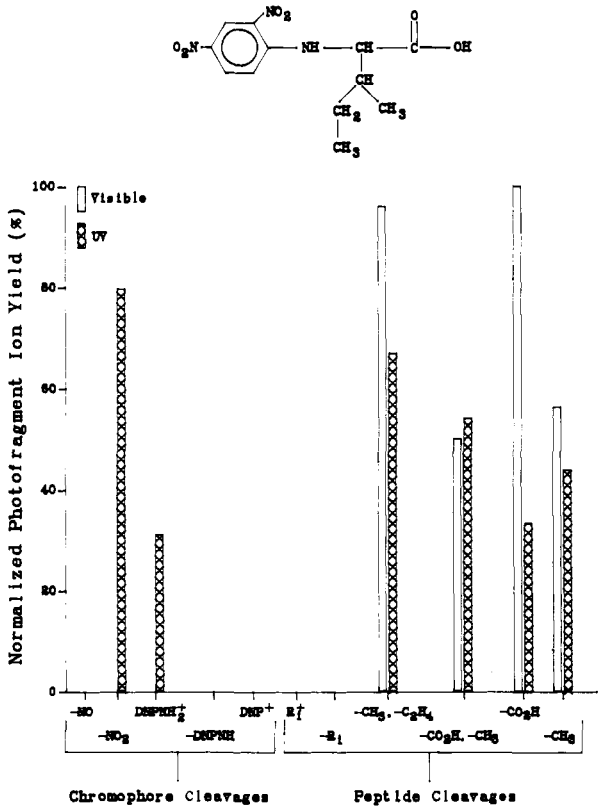

Figure 7. Photofragment ion histogram of DNP-isoleucine. Photodissociation at visible and UV wavelengths are represented by open and cross-hatched bars, respectively.

photofragment ion (see Experimental Section). In general these data follow the expected trend. That is, approximately 60% of

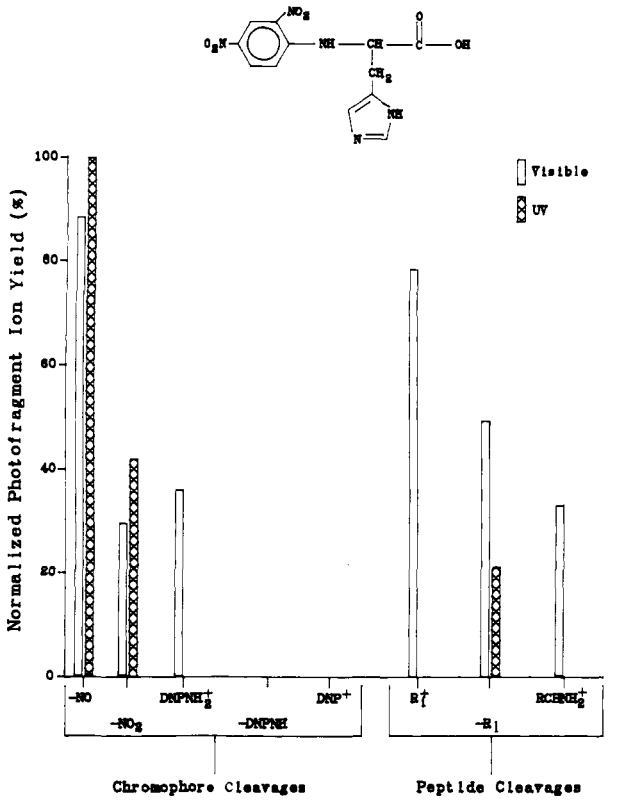

Figure 8. Photofragment ion histogram of DNP-histidine. Photodissociation at visible and UV wavelengths are represented by open and cross-hatched bars, respectively.

the DNP-glycine $[M + H]^+$ photoexcited by a visible photon dissociates promptly (with rate constants greater than ca. 6×10^6 s^{-1}). Photoexcitation with a UV photon produces a population of ions which dissociate at a greater rate; thus the observed 80–90% prompt photodissociation is reasonable. In general, this same trend is observed throughout the data set; i.e., a larger fraction of the photoexcited ions dissociates promptly by UV excitation, and the percentage of prompt dissociation decreases as the size of the molecule increases. There are additional trends in the data that should be noted: (i) some photodissociation reactions, e.g., loss of CH_3 and CO_2H from DNP-leucine and DNP-isoleucine, are relatively slow reactions; (ii) for the DNP amino acids the percentage of prompt dissociation for visible photoexcitation is significantly smaller than for UV photoexcitation; (iii) for the DNP dipeptides the percentage of prompt dissociation is approximately the same for visible and UV photoexcitation; and (iv) for the DNP tripeptides visible photoexcitation yields exclusively slow photodissociation.

Discussion

The visible and UV photodissociation data for DNP-glycine (Table I) illustrate many of the general trends observed in the photodissociation of the DNP amino acids. Photodissociation of the $[M + H]^+$ ions of DNP-glycine at visible wavelengths leads exclusively to cleavages within the glycyl group, e.g., loss of CO_2H and OH. By contrast, the UV photodissociation of DNP-glycine results in dissociation reactions involving the chromophore and the glycyl residue. The same general trend is observed for DNP-alanine. For example, loss of NO_2 and cleavage of the -NH-CH- bond to form the DNP-NH_2^+ ion are only observed by UV excitation.

In general, photofragmentation of the DNPNH–peptide bonds results in charge retention by the N-terminus fragment; however, exceptions to this trend are observed for DNP amino acids which contain basic or aromatic R groups, viz., histidine and tryptophan. For example, the dominate reaction channel observed in the photofragment ion spectrum of DNP-tryptophan $[M + H]^+$ ion, using either visible or UV photons, is loss of DNPNH (charge retention by the tryptophan residue). Biemann and Martin have

Table I. Photodissociation Kinetic Data, Normalized Metastable, CID, and Photofragment Ion Yields for the $[M + H]^+$ Ions of DNP Amino Acids

	visible	photodissociation		UV		CID		M*	
cleavage	RI (%)	$I/\sum I$(%)	prompt (%)	RI (%)	$I/\sum I$ (%)	prompt (%)	RI (%)	$I/\sum I$ (%)	RI (%)	$I/\sum I$ (%)
DNP-glycine										
$-NO_2$				63	26	90	69	18	46	27
$-CH_2CO_2H$				58	24	75				
$-CO_2H$	31	24	60	100	41	80	25	6	9	5
-OH	100	76	55	21	9	80	100	26	100	59
DNP-alanine										
$-NO_2$				26	11	75	92	20	71	39
$DNPNH_2^+$				38	16	70	8	2		
$-CO_2H$, $-CH_3$	67	29	35	100	42	60	71	16	3	2
$-CO_2H$	63	28	50	51	22	70	34	7	4	2
$-CH_3$	100	43	45	22	9	70	100	22	100	55
DNP-β-alanine										
$-CH_2CO_2H$	100	51	35	100	75	60	100	34	100	57
-OH	95	49	60	33	25	75	81	27	66	37
DNP-valine										
$-NO_2$				100	27	70	22	5		
$-CO_2H$, $-CH_3$	18	8	30	58	16	50	75	17		
$-CO_2H$	40	17	35	72	20	55	100	23	88	47
$-CH_3$	100	43	35	73	20	65				
-OH	74	32	40	63	17	65	98	22	100	53
DNP-leucine										
$-NO_2$				80	33	55	13	3		
DNP^+				15	6	50	11	2		
$-CO_2H$, $-CH_3$	60	26	20	27	11	35	73	16		
$-CO_2H$	100	43	30	100	41	40	98	22	84	45
$-CH_3$	71	31	30	23	9	50				
DNP-isoleucine										
-NO				100	26	50	16	4		
$DNPNH_2^+$				39	10	45	10	2		
$-CH_2CH_2CH_3$	96	32	25	84	22	40				
$-CO_2H$, $-CH_3$	50	17	20	68	17	35	68	15		
$-CO_2H$	100	33	30	42	11	45	100	22	100	53
$-CH_3$	56	18	30	55	14	45				
DNP-histidine										
-NO	100	29	25	100	61	40	10	2		
$-NO_2$	33	9	45	42	26	55				
$DNPNH_2^+$	41	12	40				14	3		
R^+	79	23	40				72	17		
-R	56	16	35	21	13	50	14	3		
$RCHNH_2^+$	37	11	30				10	2		
DNP-phenylalanine										
$-NO_2$				100	30	45	19	2		
$-NO_2$, -OH				24	7	35	53	6		
-DNPNH	33	15	20	49	15	40				
$DNPNHCH_2^+$				30	9	30	80	8		
R^+	18	8	25	24	7	35	93	11		
-R				36	11	35	60	7		
-R-OH	26	11	30							
$-CO_2H$	49	22	20				100	12	100	54
-OH	100	44	25	72	21	40	67	8		
DNP-tryptophan										
$-NO_2$, -OH				27	17	40				
-DNPNH	100	71	35	100	65	50	100	46	100	66
R^+	41	29	30	28	18	45	90	42	10	7

discussed the relationship between site of protonation and bond cleavage reactions,[28] and the collision-induced dissociation reactions of model tri- and tetrapeptide $[M + H]^+$ ions have been explained in terms of site of protonation.[29] The stabilities and low heats of formation of aromatic R groups favor production of the R^+ ion. Note that the R^+ photofragment ion is only observed for DNP-phenylalanine, DNP-tryptophan, and DNP-histidine. Note, also, that the R^+ photofragment ion is formed by visible photodissociation of DNP-histidine, but is not observed as a UV fragment ion.

The loss of small neutrals, e.g., $OH^•$, $CH_3^•$, and $CO_2H^•$, from the DNP amino acids and peptides are important visible photodissociation reaction channels. For example, the dominant visible photofragment ion observed for DNP-phenylalanine $[M + H]^+$ (see Figure 5) is loss of OH. Likewise, loss of CO_2H from the $[M + H]^+$ ion of DNP-leucine and DNP-isoleucine is the base peak in the visible photofragment ion spectra (see Figures 6 and 7, respectively). These same small neutral losses are important fragment ions in the CID and unimolecular spectra as well (see Table I). Important differences between the visible photodissociation data and the CID data are evident; e.g., CID produces extensive fragmentation throughout the peptide backbone and chromophore which is not observed by visible photodissociation.

It is interesting to note that the UV photodissociation of several of the DNP amino acids and DNP peptides result in a decreased number of peptide cleavages (relative to visible photodissociation). For example, Figure 8 contains the photofragment ion data for the $[M + H]^+$ ion of DNP-histidine. Note that only three fragment ions are observed by UV photodissociation: $[M + H]^+ - NO$, $[M + H]^+ - NO_2$, and $[M + H]^+ - R$ ($R = CH_2$-

(28) Blemann, K.; Martin, S. A. *Mass Spectrom. Rev.* **1987**, *6*, 1.
(29) Mallis, L. M.; McGlohon, E.; Russell, D. H. *Anal. Chem.* **1988**, *60*, 1818.

Table II. Photodissociation Kinetic Data, Normalized Metastable, CID, and Photofragment Ion Yields for the $[M + H]^+$ Ions of DNP Dipeptides

		visible	photodissociation		UV		CID		M*	
cleavage	RI (%)	$I/\Sigma I$ (%)	prompt (%)	RI (%)	$I/\Sigma I$ (%)	prompt (%)	RI (%)	$I/\Sigma I$ (%)	RI (%)	$I/\Sigma I$ (%)
DNP-glyclalanine										
$-NO_2$	100	32	35	100	58	35	91	18	40	22
A_1	39	13	25	34	20	30	100	20	1	1
Y_1	65	21	20	38	22	30	74	15	7	4
B_1, $-NO_2$	27	9	30				37	7		
$-CO_2H$	79	25	25				32	6	16	9
DNP-glycyl-β-alanine										
$-NO$				25	18	25				
$-NO_2$	62	19	35				19	6	18	14
$DNPNH_2^+$	39	12	30				21	7		
A_1	100	30	25	15	11	30	65	20		
Y_1	31	9	20				25	8	3	2
B_1, $-NO_2$	36	11	30							
$-CO_2H$	64	19	25				23	7	8	6
$-OH$				100	71	20	100	31	100	78
DNP-glycylvaline										
$-NO$				100	54	20				
$-NO_2$	78	21	20				100	30		
$-NO$, $-NO_2$				11	6	20				
DNP^+				6	3	30	7	2		
$-R_2$	38	10	15							
A_1	31	8	15	17	9	25	59	18		
Y_1	66	17	15	23	13	30	29	9		
C_1				19	10	25				
B_1–NO_2	63	17	20	9	5	30	25	8		
$-CO_2H$	100	27	15				31	9	100	69

Table III. Photodissociation Kinetic Data, Normalized Metastable, CID, and Photofragment Ion Yields for the $[M + H]^+$ Ions of DNP Tripeptides

		visible	photodissociation		UV		CID		M*	
cleavage	RI (%)	$I/\Sigma I$ (%)	prompt (%)	RI (%)	$I/\Sigma I$ (%)	prompt (%)	RI (%)	$I/\Sigma I$ (%)	RI (%)	$I/\Sigma I$ (%)
DNP-prolylleucylglycine										
A_1				28	16	15	96	35	2	1
B_2	100	96	0	100	55	10	100	36	100	92
A_1–NO_2	4	4	0	11	6	15	16	6		
$-OH$				41	23	15			4	3
DNP-propylglutaminylglycine										
$-NO$				87	26	10				
A_1	8	4	0	43	13	10	100	24	3	1
B_2	63	33	0	100	30	15	90	22	100	50
C_1				20	6	10				
A_1–NO_2	14	7	0	25	7	15	31	8		
B_1–NO_2				23	7	15	35	9		
C_1–NO_2	8	4	0	35	11	10				
$-OH$	100	52	0				96	23	91	46

imidazole). Formation of the $RCHNH_2^+$ ion (m/z 110), a fragment ion indicative of the histidine residue, is observed by CID and visible photodissociation, but the m/z 110 ion is absent in the UV photodissociation spectrum. In addition, loss of NO and NO_2 dominate the UV photofragment ion spectrum (i.e., $I/\Sigma I$ = 87% for these two reaction channels) for DNP-histidine.

Cleavages within the dinitrophenyl group are also important photodissociation reaction channels for the DNP di- and tripeptides in Tables II and III, respectively. For example, loss of NO_2 is the dominate reaction channel for DNP-glycylalanine (visible and UV photoexcitation), and loss of NO dominates the UV photofragment ion spectra of DNP-glycylvaline and DNP-prolylglutaminylglycine. The A_1 and Y_1 cleavage reactions are observed for all DNP dipeptides. The ($I/\Sigma I$) values for the A_1 and Y_1 photofragment ions are generally larger for visible photoexcitation (as compared with UV photoexcitation). The B_2 cleavage is an important reaction channel for the DNP tripeptides. The B_2 photofragment ion is the base peak for the UV photoexcitation of DNP-prolylleucylglycine and DNP-prolylglutaminylglycine. An important difference between photodissociation of DNP amino acids and DNP di- and tripeptides is the formation of combination peptide–chromophore cleavages. For example, the photofragment ion formed by cleavage B_1 and loss of NO_2 (denoted B_1–NO_2) is observed for all three DNP dipeptides (Table II) and the cleavage reactions A_1–NO_2, B_1–NO_2, and C_1–NO_2 are observed in the photofragment ion spectrum for DNP-prolylglutaminylglycine (Table III).

Comparison of the CID and UV photodissociation spectra reveal some interesting differences. The major difference is the enhanced chromophoric cleavages (especially loss of NO and NO_2) observed by UV photodissociation. For example, loss of NO or NO_2 is a major reaction channel by UV photoexcitation of DNP-valine, DNP-isoleucine, DNP-histidine, DNP-phenylalanine, DNP-glycylalanine, and DNP-glycylvaline $[M + H]^+$ ions (see Tables I and II). Although the NO and NO_2 losses are observed in the CID spectra of DNP peptides, these reaction channels represent a small fraction of the total ion yield, e.g., $I/\Sigma I$ = 3%, 4%, and 2% for loss of NO_2 for DNP-leucine, DNP-isoleucine, and DNP-phenylalanine, respectively. We observe similar results for the photodissociation of dansyl derivatized peptides; i.e., photodissociation at 350 nm yields exclusively cleavages within the dansyl group and no peptide cleavage reactions are observed.[30] Note, also, that loss of CH_2CO_2H is an important UV photofragment ion for DNP-glycine, but this reaction channel is not observed by CID or metastable reactions. Similarly, loss of C_3H_7 for the DNP-isoleucine $[M + H]^+$ ion is an important photo-

(30) Tecklenburg, R. E., Jr.; Russell, D. H., unpublished results.

Scheme I

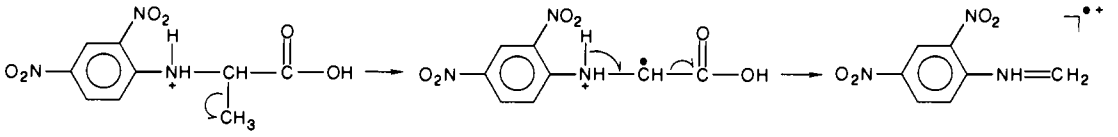

Scheme II

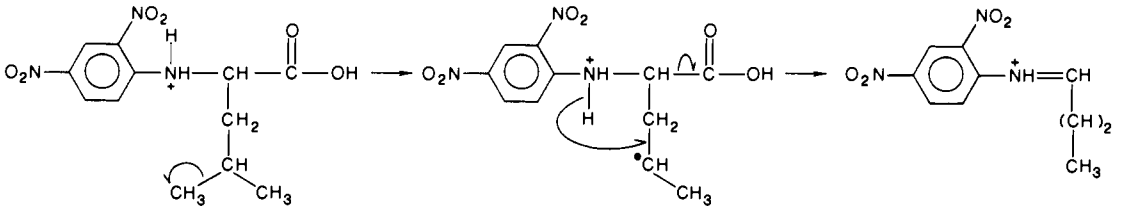

Scheme III

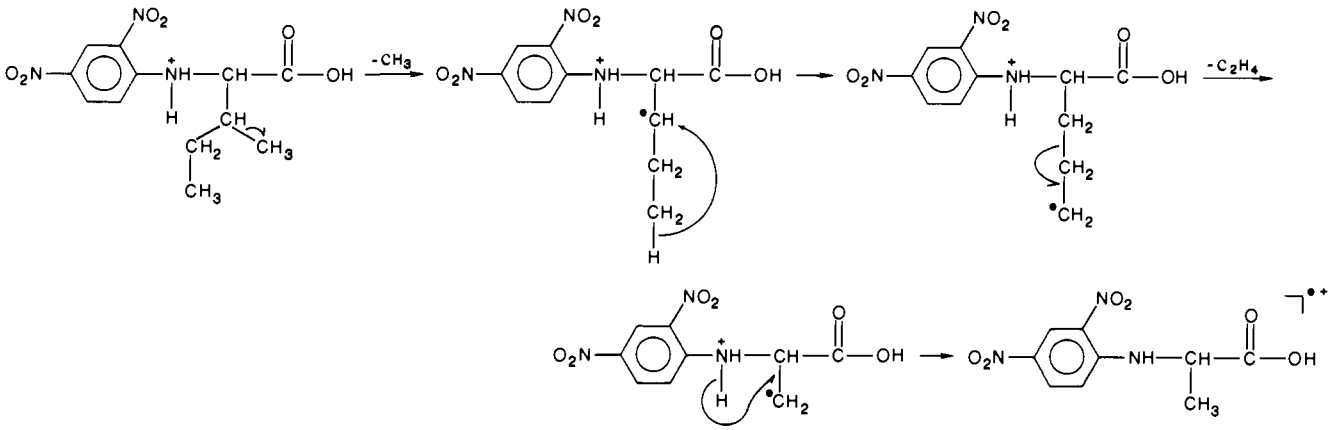

fragment ion (both visible and UV), but this reaction channel is not observed by CID. Although the relative branching ratios for various dissociation channels are different in the various spectra, this can be explained by differences in the internal energy of the dissociating ions.

One consistent trends that emerges from the photodissociation rate data is that the percentage of ions that undergo prompt dissociation rapidly decreases as the mass of incident ion is increased. For example, 55% of the DNP-glycine $[M + H]^+$ ions that fragment by loss of OH occur by prompt photodissociation. This percentage steadily decreases for larger molecular weight peptides and becomes 0 (no prompt photodissociation is observed) for loss of OH from the $[M + H]^+$ ion of DNP-prolylglutaminylglycine. This result is not surprising; i.e., as the size (degrees-of-freedom) of the molecules increases, the amount of excitation energy per degree of freedom decreases, and the rate of dissociation decreases accordingly. This effect has been discussed in terms of the reduced efficiencies for collision-induced dissociation as a function of mass.[5,31] The observed decrease in the percentage prompt dissociation is consistent with our inability to photodissociate larger peptides than reported here. We have attempted to photodissociate DNP hexapeptides and DNP heptapeptides. However, the photofragment ion yield in these experiments is below our detector sensitivity, and it is impossible to improve the S/N ratios to an acceptable level using our present experimental apparatus. Note the decreased signal-to-noise in the photofragment ion signal for the data contained in Figure 4 for the DNP amino acid, DNP dipeptide, and DNP tripeptide. It should be possible to improve the S/N ratios by increasing the photon energy or by increasing the time window for collecting the photofragment ion, e.g., detection by ICR based methods. Both of these avenues are presently being investigated.

Photodissocation Reactions Involving Distonic Radical Cations. The combined loss of CH_3 and CO_2H is an important photofragment ion for several of the DNP amino acids (e.g., DNP-alanine, DNP-valine, DNP-leucine, and DNP-isoleucine). This is an unusual cleavage reaction (unusual in terms of the "even electron rule").[32] Schemes I and II illustrate a proposed mechanism for loss of the CH_3 and CO_2H groups from the $[M + H]^+$ ions of DNP-alanine and DNP-leucine, respectively.[33] The first step of this mechanism involves loss of the methyl group which yields a distonic radical cation,[34-36] followed by a hydrogen atom transfer from the N-terminal nitrogen to the carbon radical site, followed by elimination of the C-terminal carboxylic acid group. The loss of $CH_3^\bullet$ as the first step is based on the known dissociation reactions of radical cations containing amine functional groups. For example, if CO_2H elimination occurred first, the resulting distonic radical cation could undergo an α-cleavage reaction (commonly observed for amine radical cations).[37] Thus, for DNP-valine, DNP-leucine, and DNP-isoleucine the combined loss of CO_2H and R would be expected. The fact that loss of the R group is not observed for these ions suggests that loss of the $CH_3^\bullet$ radical must precede the hydrogen transfer and CO_2H elimination steps.

Another unusual dissociation reaction involving distonic radical cations (observed for both UV and visible photoexcitation) is the

(31) Neumann, F. M.; Derrick, P. J. *Org. Mass Spectrom.* **1984**, *19*, 165.

(32) For a recent discussion of the "even-electron rule" as well as the conditions under which this rule is obeyed or violated, see: Karni, M.; Mandelbaum, A. *Org. Mass Spectrom.* **1980**, *15*, 53.

(33) Note that in both Scheme I and III the protonated precursor ions (even-electron species) eliminate radicals to produce odd-electron species which is a violation of the "even-electron rule". However, Bowen and Harrison (Bowen, R. D.; Harrison, A. G. *Org. Mass Spectrom.* **1981**, *16*, 180) have reported that loss of the methyl radical from small immonium ions is observed as an important unimolecular fragmentation reaction channel. The authors rationalized the violation of the "even-electron rule" in terms of a high stability of the radical cations ($H_f \sim 190$ kcal/mol).

(34) Yates, B. F.; Bouma, W. J.; Radom, L. *J. Am. Chem. Soc.* **1984**, *106*, 5805.

(35) Wesdemiotis, C.; Danis, P. O.; Feng, R.; Tso, J.; McLafferty, F. W. *J. Am. Soc.* **1985**, *107*, 8059.

(36) Wesdemiotis, C.; Feng, R.; McLafferty, F. W. *J. Am. Chem. Soc.* **1985**, *107*, 715.

(37) McLafferty, F. W. *Interpretation of Mass Spectra*, 3rd ed.; Turro, N. J., Ed.; University Science: Mill Valley, CA, 1980; p 218.

loss of 43 mass units (m/z 255) for the $[M + H]^+$ ions of DNP-isoleucine (m/z 298). Biemann et al. reported a collision-induced dissociation reaction corresponding to the loss of 43 mass units for peptides containing the leucine residue, and Biemann postulated that the $[M + H]^+ - 43$ fragment ion is formed by elimination of the isopropyl radical from the R group.[38] Because the isoleucine residue cannot eliminate $C_3H_7^\bullet$ without rearrangement of the butyl side chain, we propose that the DNP-leucine $[M + H]^+ - 43$ photofragment ion is formed by consecutive losses of $CH_3^\bullet$ and C_2H_4 (as opposed to loss of the propyl group ($C_3H_7^\bullet$)). The loss of $CH_3^\bullet$ and C_2H_4 from DNP-isoleucine occurs slowly with respect to other peptide and chromophore cleavages, e.g., prompt/slow (visible) = 25/75 versus 30/70 for loss of CO_2H and prompt/slow (UV) = 40/60 versus 50/50 for loss of NO_2. Again, this observation is consistent with a rearrangement reaction. Our proposed mechanism for this reaction is illustrated in Scheme III. The first step involves cleavage of the methyl group, followed by a hydrogen transfer and elimination of ethylene. Also, Biemann observes cleavage of the C_B–CH_3 bond (corresponding to $CH_3^\bullet$ loss for isoleucine-containing peptides). The fact that methyl loss is observed from both DNP-isoleucine (by photoexcitation) and isoleucine containing peptides (by collision-induced dissociation), and that subsequent loss of C_2H_4 is only observed for DNP-isoleucine, is interesting. This difference may reflect significant differences in the internal energies for the dissociating ions; i.e., the photoexcited ions probably have higher internal energies than the ions activated by collision, or that intramolecular reactions involving the radical site formed by $CH_3^\bullet$ elimination occur in the more complex peptides and thereby suppress C_2H_4 elimination.[39] We are attempting to delineate this issue by comparing the CID and photodissociation reactions of more complex DNP peptides containing the leucine and isoleucine residues.

Differentiation of Leucine and Isoleucine. Leucine and isoleucine are difficult to differentiate by mass spectrometric methods. For example, the CID spectra of the $[M + H]^+$ ions of leucine and isoleucine are identical; however, CID of the immonium ion (R–CH–NH_2^+; m/z 86) results in slight differences in the relative abundances of the fragment ions.[40,41] By contrast, comparison of the photofragment ion histograms for the $[M + H]^+$ ion of DNP-leucine (Figure 6) and DNP-isoleucine (Figure 7) reveal significant differences. The major difference is for loss of CH_3 and C_2H_4 from the $[M + H]^+$ ion of DNP-isoleucine. Note that this same reaction channel is not observed for DNP-leucine. Likewise, loss of the CH_3 and C_2H_4 from the $[M + H]^+$ ions of DNP-leucine or DNP-isoleucine and leucine or isoleucine is not observed by CID or metastable dissociation (see Table I). Another difference between the leucine and isoleucine photodissociation spectra is formation of the $DNPNH_2^+$ ion which is observed for UV photoexcitation of DNP-isoleucine. These results suggest that the higher selectivity available in the photodissociation technique (as compared to CID) can be useful in distinguishing structural isomers.

Gas-Phase Photochemistry of Ionized Peptides and Related Molecules. The question arises as to what factors govern the dissociation reactions of highly functionalized complex molecules such as $[M + H]^+$ ions of peptides. As noted above, one important factor that influences the dissociation reactions of peptides is the site of protonation.[15,29] On the other hand, photodissociation may be a more complicated process. In particular, photoexcitation produces a population of photoexcited ions with a narrow distribution of internal energies, and photoexcitation may initially occur remote from the charge site; e.g., the proposed mechanism for formation of distonic radical cations is a type of remote-site fragmentation.

McIver et al. have reported that small peptides containing aromatic residues readily photodissociate (at 193 nm) and the major photofragment ions observed are those formed by bond cleavages at or near the amide groups.[42,43] For larger peptides similar photodissociation reactions are observed; Hunt has reported the photodissociation products of a 15-residue tryptic peptide.[44] In this particular case, the entire series of Y_i fragments are observed, and the sequence obtained is consistent with that obtained by Edman degradation. Lubman and Tembreull have also studied the fragmentation reactions of model peptides and related molecules ionized by multiphoton ionization (266 and 280 nm).[45-47] Lubman's MPI mass spectra contain relatively few fragment ions, and the spectra are typically dominated by a single fragment ion. For example, the dominant photofragment ion formed by MPI of phenylalanyltyrosine[48] is m/z 107 ($C_7H_7O^+$), i.e., the tyrosine R group (R = *p*-hydroxybenzyl). Similarly, photodissociation of DNP-phenylalanine $[M + H]^+$ ion yields the R^+ ion ($C_7H_7^+$) and loss of R ($C_7H_7^\bullet$) as important photofragments. Note, that the $C_7H_7O^+$ ion is quite stable ($H_f \sim 173$ kcal/mol)[49] as is the $C_7H_7^+$ ion ($H_f \sim 212$ kcal/mol); consequently one can imagine that formation of these ions would be a favorable relaxation process. The formation of R^+ ions by photodissociation of DNP-histidine and DNP-tryptophan $[M + H]^+$ can be rationalized by a similar argument. Although McLafferty has proposed that photofragment ions of model peptides appear to be associated with specific absorption and dissociation, the results are probably due to formation of stabilized ions.[50] For example, McIver reported a prominent photofragment ion at m/z 120 ($NH_2{=}CHCH_2C_6H_5$) for photodissociation of glycylphenalanylalanine $[M + H]^+$ ions. The m/z 120 fragment ion is the commonly observed phenylalanyl immonium ion,[51] which is often observed as a amino acid specific ion. Therefore, the phenylalanyl immonium ion that is formed upon photoexcitation is probably not an energy specific fragment ion.

In some cases photodissociation of DNP amino acids and DNP peptides favors loss of NO or NO_2, especially for UV photodissociation. For example, loss of NO_2 from the $[M + H]^+$ ions of DNP-glycine, DNP-valine, DNP-leucine, DNP-isoleucine, and DNP-phenylalanine, and loss of NO from the $[M + H]^+$ ion of DNP-histidine are dominate photodissociation reactions channels at 350 nm. Not that these same chromophoric cleavages are often not observed in the visible photofragment ion spectra. We attribute such differences in the photodissociation reactions to kinetic effects. Specifically, photon absorption produces excited $[M + H]^+$ ions with a relatively narrow distribution of internal energies, and at this particular internal energy a single dissociation reaction channel dominates the unimolecular chemistry. Similar observations have been reported by other workers. For example, Chen and Dunbar reported that photodissociation of *n*-heptane ions yield $C_4H_9^+$ and $C_3H_7^+$ photofragment ions.[52] The abundance of the $C_3H_7^+$

(38) Johnson, R. S.; Martin, S. A.; Biemann, K.; Stults, J. T.; Watson, J. T. *Anal. Chem.* **1987**, *59*, 2621.

(39) A referee raised a question concerning the absence of $C_2H_5^\bullet$ loss from DNP-isoleucine; i.e., loss of both $CH_3^\bullet$ and $C_2H_5^\bullet$ should be competitive with loss of the latter favored thermodynamically. This question cannot be fully answered until the dissociation reaction mechanism has been studied in more detail; however, it is rather likely that the driving force for loss of $CH_3^\bullet$ is product ion stability, as noted by Bowen and Harrison.[33]

(40) Aubagnac, I. L.; Amrani, B. E.; Devienne, F. M.; Combarieu, R. *Org. Mass Spectrom.* **1985**, *20*, 429.

(41) Johnson, R. S.; Martin, S. A.; Biemann, K.; Stults, J. T.; Watson, J. T. *Anal. Chem.* **1987**, *59*, 2621.

(42) Bowers, W. D.; Delbert, S. S.; Hunter, R. L.; McIver, R. T., Jr. *J. Am. Chem. Soc.* **1984**, *106*, 7288.

(43) Bowers, W. D.; Delbert, S. S.; McIver, R. T., Jr. *Anal. Chem.* **1986**, *58*, 969.

(44) Hunt, D. F.; Shabanowitz, J.; Yates, J. R., III *J. Chem. Soc., Chem. Commun.* **1987**, 548.

(45) Tembreull, R.; Lubman, D. M. *Anal. Chem.* **1987**, *59*, 1082.

(46) Tembreull, R.; Lubman, D. M. *Anal. Chem.* **1987**, *59*, 1003.

(47) Tembreull, R.; Lubman, D. M. *Appl. Spectrosc.* **1987**, *41*, 431.

(48) Tembreull, R.; Lubman, D. M. *Anal. Chem.* **1987**, *59*, 1003.

(49) Russell, D. H.; Freiser, B. S.; McBay, E. H.; Canada, D. C. *Org. Mass Spectrom.* **1983**, *18*, 474.

(50) McLafferty F. W.; Amster, I. J.; Furlong, J. J. P.; Loo, J. A.; Wang, B. H.; Williams, E. R. *Fourier Transform Mass Spectrometry*; Buchanan, M. V., Ed.; American Chemical Society: Washington D.C., 1987; Vol. 359, pp 116.

(51) Bertrand, M. J.; Thibault, P. *Biomed. Environ. Mass Spectrom.* **1986**, *13*, 347.

(52) Chen, J. H.; Dunbar, R. C. *Int. J. Mass Spectrom. Ion Proc.* **1986**, *72*, 115.

fragment ion is found to increase dramatically with increasing photon energy (2.1–3.5 eV). The authors postulate that the behavior of this system is a consequence of energy-specific dissociation; i.e., photon absorption produces ions in an energy regime dominated by a rapid and specific dissociation channel. Chang and Johnston made similar observations for MPI and dissociation reactions of C_7H_8O and $C_8H_{10}O$ isomers and noted that the product ions show a strong dependence upon the excitation wavelength.[53] These results are explained in terms of a narrow internal energy distribution for the ions, and these ions subsequently dissociate by energy specific pathways. This point is illustrated in Figure 1; note that the narrow internal energy distribution for the photoexcited ion imposes a limit on the available dissociation reactions.

Kinetic data for the photodissociating ions are useful for understanding the differences in the photofragment ion spectra. As noted above, the fraction of prompt dissociation reactions decreases on going from UV to visible photoexcitation; in some cases this trend is very dramatic. For example, NO_2 loss from DNP-glycine $[M + H]^+$ ions is not observed by visible photoexcitation; however, upon UV photoexcitation, NO_2 loss is the dominant reaction channel and the ratio for prompt/slow photofragment ions is approximately 90/10. Thus, by UV photoexcitation the NO_2 loss reaction channel is dominant and the rate of the dissociation reaction is quite large. The data for NO and NO_2 loss from DNP-histidine $[M + H]^+$ ion is another interesting example. Note that for both visible and UV photoexcitation the percentage of prompt NO loss is less than for NO_2 loss, e.g., 25% versus 40% for visible photoexcitation and 40% versus 55% for UV photoexcitation. These data suggest that NO loss is an inherently lower energy reaction than NO_2 loss. The mechanism for NO loss from nitro aryls has been studied extensively, and it is generally believed to involve a slow rearrangement reaction.[54] Thus, our data are consistent with a kinetic shift for the photodissociation reaction involving NO loss. It is also of interest to note that the only $[M + H]^+$ ion that loses NO by visible photoexcitation is DNP-histidine. On the basis of collision-induced dissociation data, we have proposed that protonation at the imidazole N of histidine is stabilized by secondary interactions such as illustrated by structure II.[16] It could be argued, therefore, that NO loss from

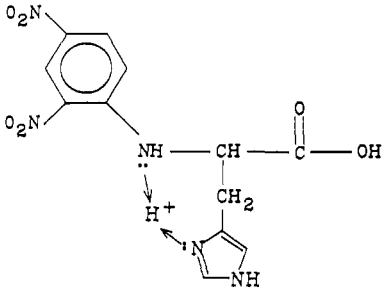

II

DNP-histidine $[M + H]^+$ ions is promoted by interaction between the ortho NO_2 group and the charge localization inferred from structure II. We are testing this hypothesis by examining additional model systems which alter the charge distribution at the N-terminal nitrogen and the chromophore.

Several additional interesting observations arise upon close inspection of the photodissociation rate data. Loss of the NO_2 group from the DNP amino acids and peptides is always observed to occur quickly with respect to peptide cleavages of the same molecules. For example, the ratio for prompt/slow NO_2 loss for DNP-valine $[M + H]^+$ ions is 70/30, whereas the prompt/slow ratio for CO_2H loss is 55/45. This result suggests that photoexcited DNP-valine $[M + H]^+$ ions which dissociate with lifetimes of less than 1.4×10^{-7} s favor loss of NO_2, but the long-lived ions favor loss of CO_2H. Thus, it would appear that loss of NO_2 is the kinetically favored reaction channel and loss of CO_2H yields the thermodynamically favored product ion. There are very few experimental data to corroborate this hypothesis; however, competition between kinetic and thermodynamically controlled reactions have been studied by field ionization kinetics.[55] There are numerous examples where the ionic products from a unimolecular reaction change as the lifetime (and presumably internal energy) of the dissociating ion changes.

Conclusions

Dissociation of amino acids and small peptides can be accomplished by low-energy UV (350 nm) and visible photoexcitation using a dinitrophenyl chromophore attached to the N-terminus. Although such derivatization procedures may not provide the most viable analytical approach for structural characterization of complex biomolecules, there are particular advantages of the method for studies of the dissociation reaction of such systems. Specifically, photon absorption by the chromophore produces an ion with a known amount of internal energy, and the photofragment ions formed and the relative branching ratios among the available reaction channels yield information on the dissociation energetics for the ion. Although there are clear indications that all energetically accessible photofragment ions are formed, kinetic data for the photofragment ions reveal that some reaction channels are subject to considerable kinetic shifts. In addition, at higher excitation energy (350 nm) there are clear preferences for dissociation reactions involving the chromophore, specifically loss of NO or NO_2. Although it may be possible to eliminate competing dissociation reaction channels by the use of a more robust chromophore, careful consideration must be given to the selection of the chromophore. For example, we have preliminary data for the dansyl chromophore which shows that chromophoric cleavages of this system attenuate the photofragment ion yields involving fragmentation of the peptide.

A particularly interesting observation of this study is the importance of photodissociation reactions which yield odd-electron ions from the even-electron precursors. For example, loss of $CH_3^\bullet$ or $COOH^\bullet$ are important photodissociation reactions of the $[M + H]^+$ ions of DNP amino acids and DNP peptides. These reactions are explained in terms of formation of distonic radical cations, and, in fact, it is demonstrated that such reactions can be used to differentiate DNP-leucine and DNP-isoleucine $[M + H]^+$ ions.

Future work in this area will be directed toward detailed studies on the photochemistry of more complex peptides and the influence of the chromophore on the observed photochemistry. For example, we have found that photoexcitation of peptide $[M + H]^+$ ions containing the dansyl chromophore (attached to the N-terminus) yields distinctively different photofragment ions than for the dinitrophenyl chromophore. Also, the absolute photofragment ion yields (involving fragmentation of the peptide) are different for the two chromophores; the yield is always much higher (by a factor of 2–5) for DNP than for dansyl derivatized peptides. The photochemistry of the DNP peptides shows a rather strong positional dependence on the chromophore which must be studied further. For example, the DNP group can be attached to small peptides containing arginine at either the N-terminus or the guanidyl N, and the photofragment ions (and photofragment ion yields) formed by these two isomers are different. Our preliminary interpretation of this result is that the differences can be attributed to a preference for remote-charge site fragmentation in the case of N-terminus attachment of DNP, whereas charge-site fragmentation is preferred when the DNP group is attached to the guanidyl N of arginine.

It is quite clear that detailed information on the dissociation reactions of peptide $[M + H]^+$ ions can be obtained by the methods described in this paper. Using the methods described, both energetic and kinetic data can be used to probe the disso-

(53) Chang, T. C.; Johnston, M. V. *J. Phys. Chem.* **1987**, *91*, 884.
(54) Cooks, R. G.; Beynon, J. H.; Ast, T. *J. Am. Chem. Soc.* **1972**, *94*, 1004.
(55) Levsen, K. *Fundamental Aspects of Organic Mass Spectrometry*, Verlag Chemie: Weinheim, 1978; pp 194–196, (see also pp 234–237).

ciation reactions of relatively complex biomolecules. In addition, detailed questions on the factors which govern the dissociation chemistry of these systems can be obtained by appropriate choice and positioning of the chromophoric group.

Acknowledgment. This work was supported by grants from the U.S. Department of Energy, Division of Chemical Sciences, Office of Basic Energy Sciences (DE-AS05-82ER13023), and the National Science Foundation (CHE-8418457).

Registry No. DNP-Gly-OH, 1084-76-0; DNP-Ala-OH, 1655-52-3; DNP-β-Ala-OH, 3185-97-5; DNP-Val-OH, 1694-97-9; DNP-Leu-OH, 1655-57-8; DNP-Ile-OH, 1655-56-7; DNP-His-OH, 10457-26-8; DNP-Phe-OH, 1655-54-5; DNP-Trp-OH, 1655-51-2; DNP-Gly-Ala-OH, 58979-22-9; DNP-Gly-β-Ala-OH, 118439-08-0; DNP-Gly-Val-OH, 58979-23-0; DNP-Pro-Leu-Gly-OH, 65985-66-2; DNP-Pro-Gln-Gly-OH, 65080-33-3.

Tunneling in Spin-State Interconversion of Ferrous Spin-Crossover Complexes: Concentration Dependence of Apparent Activation Energy Determined in Solution by Laser-Flash Photolysis

Andrew J. Conti, Chuan-Liang Xie, and David N. Hendrickson*

Contribution from the School of Chemical Sciences, University of Illinois, Urbana, Illinois 61801. *Received June 21, 1988*

Abstract: The pulsed-laser photolysis technique is used to monitor the relaxation from the high-spin state ($^5T_2$) to the low-spin ground state ($^1A_1$) of a series of Fe^{II} spin-crossover complexes. The hexadentate ligand is the Schiff base condensate from the reaction of x moles of 6-methyl-2-pyridinecarboxaldehyde, y moles of 2-pyridinecarboxaldehyde, and 1 mole of tris(2-aminoethyl)amine (tren), which gives complexes of the composition $[Fe(6\text{-Me-py})_x(py)_y tren](ClO_4)_2$. Complex **1** ($x = 3, y = 0$) is high-spin in acetone at room temperature, complex **4** ($x = 0, y = 3$) is low-spin, and complexes **2** ($x = 2, y = 1$) and **3** ($x = 1, y = 2$) have both high- and low-spin complexes in equilibrium in acetone at room temperature. At $\sim 5 \times 10^{-4}$ M in acetone, the complexes **2**, **3**, and **4** give $^5T_2 \rightarrow {}^1A_1$ relaxation rate constants (k), which for each complex in the range of 180–300 K give linear ln k versus $1/T$ plots. Apparent Arrhenius activation energies (slopes of the line) are found to be 1029 (19) cm^{-1} for **2**, 870 (15) cm^{-1} for **3**, and 648 (12) cm^{-1} for **4**. Variable-temperature relaxation data are also presented for complex **2** at $\sim 5 \times 10^{-4}$ M in acetonitrile, dichloromethane, methanol, and (2:1) toluene/acetonitrile. The apparent activation energy for complex **2** is found to be solvent dependent with values of 1310 (34) cm^{-1} for acetonitrile, 1170 (23) cm^{-1} for dichloromethane, 1080 (24) cm^{-1} for methanol, and 1010 (20) cm^{-1} for (2:1) toluene/acetonitrile. In an effort to understand the factors determining these energies the concentration dependence of the activation energy for complex **4** was determined from 0.0539 to 0.500 mM in acetone. The activation energy for the $^5T_2 \rightarrow {}^1A_1$ conversion decreases linearly with increasing concentration from 1072 (28) cm^{-1} at 0.0539 mM to 649 (12) cm^{-1} at 0.500 mM. Electrical conductivity measurements for complexes **2**, **3**, and **4** in acetone show that the level of ion pairing (aggregation) is changing throughout the ~0.05 to 0.5 mM range. Fitting of the relaxation data to Hopfield's theoretical model for tunneling between two weakly interacting states indicates that ion pairing affects the zero-point energy difference (ΔE_0) between the $^5T_2$ and $^1A_1$ states. As the concentration of complex **4** in acetone is increased, ΔE_0 increases. The tunneling rate for the complex converting from a given vibrational level of the $^5T_2$ state to a vibrational level which is of similar energy in the $^1A_1$ potential well increases as ΔE_0 increases.

In a recent paper[1] the pulsed-laser photolysis technique was employed to monitor in the 300 to 4.2 K range the relaxation rate from the high-spin state ($^5T_2$) to the low-spin state ($^1A_1$) of a Fe^{II} spin-crossover complex doped in polystyrene sulfonate. It was found that at temperatures below ~120 K the relaxation rate becomes relatively independent of temperature with a value of 1.4 (±0.5) $\times 10^4$ s^{-1} in the 50–4.2 K range. This lack of temperature dependence of the rate is direct evidence that the Fe^{II} complex quantum mechanically tunnels from the $^1A_1$ to the $^5T_2$ state in the low-temperature region. Furthermore, all of the relaxation data in the 300–4.2 K range were fit to two different theoretical models for tunneling between two states. It was shown that a Boltzmann population of vibrational levels of the $^5T_2$ state, where the tunneling rate increases with an increase in vibrational quantum number, could account for an increase in the relaxation rate to 2.33×10^7 s^{-1} at 300 K. Thus, it was concluded[1] that the Fe^{II} complex was not necessarily thermally activated over a potential-energy barrier, but the Arrhenius-like behavior of the relaxation rate above ~150 K could be due to tunneling.

Several groups have investigated the spin-state interconversion phenomenon in solution using either the laser Raman[2] or ultrasonic absorption[3] temperature-jump techniques. Among other conclusions, it was found that spin-state interconversions occur faster in solution than in the solid state and that there was no concentration dependence of the kinetics.

McGarvey and co-workers[4] were the first to use the pulsed-laser photolysis technique to determine spin-state relaxation rates for spin-crossover complexes in solution. The pulsed-laser photolysis technique gives better precision in determining these rates than do the temperature-jump techniques. McGarvey et al.[4] were also able to study spin-crossover complexes in solution over a larger

(1) Xie, C.-L.; Hendrickson, D. *J. Am. Chem. Soc.* **1987**, *109*, 6981–6988.

(2) (a) Beattie, J. K.; Sutin, N.; Turner, D. H.; Flynn, G. W. *J. Am. Chem. Soc.* **1973**, *95*, 2052. (b) Dose, E. V.; Tweedle, M. F.; Wilson, L. J.; Sutin, N. *Ibid.* **1977**, *99*, 3886. (c) Hoselton, M. A.; Drago, R. S.; Wilson, L. J.; Sutin, N. *Ibid.* **1976**, *98*, 6967. (d) Petty, R. H.; Dose, E. V.; Tweedle, M. F.; Wilson, L. J. *Inorg. Chem.* **1978**, *17*, 1064. (e) Dose, E. V.; Murphy, K. M.; Wilson, L. J. *Ibid.* **1976**, *15*, 2622. (f) Reeder, K. A.; Dose, E. V.; Wilson, L. J. *Ibid.* **1978**, *17*, 1071. (g) Dose, E. V.; Hoselton, M. A.; Sutin, N.; Tweedle, M. F.; Wilson, L. J. *J. Am. Chem. Soc.* **1978**, *100*, 1142.

(3) (a) Beattie, J. K.; Binstead, R. A.; West, R. J. *J. Am. Chem. Soc.* **1978**, *100*, 3044. (b) Binstead, R. A.; Beattie, J. K.; Dewey, T. G.; Turner, D. H. *Ibid.* **1980**, *102*, 6442.

(4) (a) Lawthers, I.; McGarvey, J. I. *J. Am. Chem. Soc.* **1984**, *106*, 4280. (b) McGarvey, J. I.; Lawthers, I.; Toftlund, H. *J. Chem. Soc., Chem. Commun.* **1984**, 1576. (c) McGarvey, J. J.; Lawthers, I. *Ibid.* **1982**, 906.

0002-7863/89/1511-1171$01.50/0